Speeding up Dynamics by Tuning the Noncommensurate Size of Rodlike Particles in a Smectic Phase

Massimiliano Chiappini,[1,*] Eric Grelet,[2] and Marjolein Dijkstra[1,†]
[1]Soft Condensed Matter, Debye Institute for Nanomaterials Science, Department of Physics, Utrecht University, Princetonplein 1, Utrecht 3584 CC, The Netherlands
[2]Centre de Recherche Paul-Pascal, UMR 5031, CNRS & Université de Bordeaux, 115 Avenue Schweitzer, 33600 Pessac, France

(Received 5 December 2019; accepted 4 February 2020; published 26 February 2020)

Using simulations, we study the diffusion of rodlike guest particles in a smectic environment of rodlike host particles. We find that the dynamics of guest rods across smectic layers changes from a fast nematiclike diffusion to a slow hopping-type dynamics via an intermediate switching regime by varying the length of the guest rods with respect to the smectic layer spacing. We determine the optimal rod length that yields the fastest and the slowest diffusion in a lamellar environment. We show that this behavior can be rationalized by a complex 1D effective periodic potential exhibiting two energy barriers, resulting in a varying preferred mean position of the guest particle in the smectic layer. The interplay of these two barriers controls the dynamics of the guest particles yielding a slow, an intermediate, and a fast diffusion regime depending on the particle length.

DOI: 10.1103/PhysRevLett.124.087801

Understanding the dynamics of particles or objects in crowded environments is important in many fields ranging from traffic jams [1], evacuations of crowds, sheep herding, evasive tumor growth, to caging in colloidal glasses [2–4]. The motion of a guest particle in a disordered crowded environment is severely hampered by its surrounding constituents. As most disordered systems are characterized by only one relevant length scale (e.g., particle size), a simple picture emerges: the bigger the particle the slower its dynamics [5–8]. This phenomenon is invariant across scales as demonstrated by the above-mentioned examples. However, this simple picture breaks down as the environment becomes inhomogeneous and ordered, yielding additional competing length scales and giving rise to remarkable exceptions to this general rule.

The motion of particles in ordered environments has been thoroughly studied in the field of liquid crystals, finding that crowded environments with different degrees of positional and/or orientational order lead to a wide variety of dynamic behaviors. For nematic liquid crystals, exhibiting long-range orientational order, the anisotropy of the environment is transferred to the motion of the particles. A fast longitudinal self-diffusion is observed in the direction parallel to the nematic director $\hat{\mathbf{n}}$ (the average particle orientation), and a slow transverse self-diffusion in the perpendicular direction [9–11].

In the case of long-range positional order, the dynamics strongly depends on the dimensionality of the translational order and the corresponding effective energy landscape. In 3D colloidal crystals, particles are confined to their lattice positions, and the diffusion is largely determined by the motion of defects [12–14]. In columnar liquid crystals, showing 2D positional order, a liquidlike longitudinal diffusion is observed within the columns, accompanied by a transverse hopping-type dynamics between different columns [15,16]. Finally, in smectic liquid crystal phases characterized by a quasi-long-range 1D translational order, a quantized hopping-type dynamics is found across smectic layers as the particles experience an effective one-dimensional periodic potential due to the lamellar organization [17–19]. Furthermore, computer simulations demonstrated cooperative motion of stringlike clusters of particles across the smectic layers [20].

In general, the presence of positional and/or orientational order introduces additional length scales to the system. In the presence of guest particles, their interplay with the various length scales associated with the structure increases the complexity of the dynamics. On the one hand, the diffusion of guest spherical particles in nematic phases of rodlike host liquid crystals has been widely addressed in literature [21–27], finding a faster diffusion in the direction longitudinal to the nematic director field. On the other hand, the diffusion of nonspherical particles in anisotropic liquid crystalline environments is still largely unexplored. Recently, Alvarez *et al.* [28] studied in experiments the diffusion of tracer amounts of noncommensurate guest viral rods in a smectic phase of shorter host fd filamentous viruses with a size ratio $L_{\mathrm{guest}}/L_{\mathrm{host}} \simeq 1.3$. Surprisingly, they found that while the host particles experience the usual hopping-type dynamics across smectic layers, the noncommensurate guest particles undergo a fast and almost continuous nematiclike diffusion, yielding the exceptional

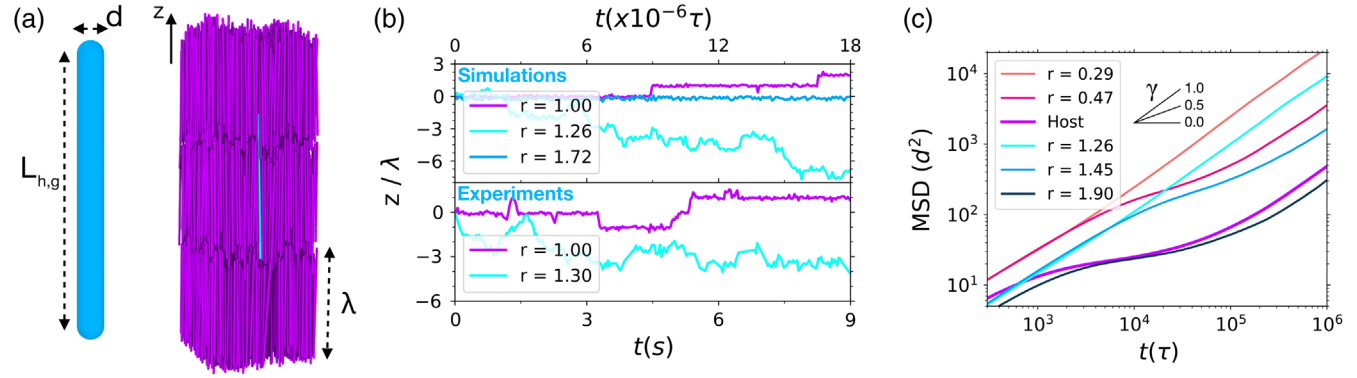

FIG. 1. (a) Snapshot from simulations of a guest spherocylinder (cyan) with cylindrical length L_g and diameter d diffusing in a host smectic phase of layer spacing λ formed by hard spherocylinders (purple) with equal diameter d and length $L_h = 40d$. (b) Example trajectories of guest particles with varying size ratio $r = (L_g + d)/\lambda$ along the nematic director $\hat{\mathbf{n}}$ of the host smectic phase in simulations (top) and experiments (bottom) [28] showing the fast nematiclike diffusion of noncommensurate guest rods with $r \sim 1.3$ and discrete hopping-type diffusion of host particles ($r \sim 1$). The conversion factor from the computational time unit τ to seconds ($\tau \sim 2 \times 10^{-6}$ s) is discussed in the Supplemental Material [31]. (c) Longitudinal mean square displacement (MSD) of simulated guest particles of varying size ratios $r = (L_g + d)/\lambda$, showing either a fast nematiclike diffusion for noncommensurate guest rods of $r \sim 1.3$ and 0.3, or a subdiffusive regime for the other guest and host particles. The diffusion exponents $\gamma = 0.5$ and 1 are indicated for comparison [see Eq. (1)].

case of larger guest particles diffusing faster than the smaller host ones. No significant differences between host and guest particles were found in the transverse in-layer diffusion. The typical slow hopping-type diffusion across smectic layers was recovered for dimeric and trimeric mutants of the host fd particles, namely for guest particles with length ratios of 2 and 3, respectively.

In this Letter, we study using computer simulations the dynamics of guest particles of varying lengths in a smectic environment of host particles in order to unravel the mechanism behind this highly counterintuitive fast diffusion of large noncommensurate guest particles. We show that by tuning the length of the guest rods with respect to the smectic layer spacing their longitudinal dynamics changes from a fast nematiclike diffusion to a slow hopping-type dynamics via an intermediate switching regime, thereby obtaining control over the speed and type of behavior of the longitudinal diffusion. More importantly, we determine the optimal rod size for either the fastest or slowest diffusion, and rationalize this behavior in terms of a complex 1D effective smectic periodic potential characterized by two energy barriers that each rod feels in the lamellar structure of the smectic phase. We show that the interplay and relative height of the two energy barriers control the dynamics of the guest particles, yielding a slow, an intermediate, and a fast diffusion regime depending on the particle length.

We model the experimental mixture of long and short filamentous bacteriophage viruses as a binary mixture of rigid rods. Each guest and host rod is modeled by a hard spherocylinder, i.e., a cylinder of diameter d and length L_g and L_h, respectively, capped at both ends with hemispheres of diameter d, yielding an end-to-end length of $L_{g,h} + d$ [Fig. 1(a)]. We introduce a tracer amount of $N_g = 6$ guest particles in a system of $N_h = 3072$ host particles with a length $L_h = 40d$. The overall phase sequence of isotropic, nematic, smectic-A (Sm_A), and smectic-B and/or crystal phases of fd viruses [32] is well captured by that of hard spherocylinders with $L_h = 40d$ [29], even though fd virus suspensions also display a columnar phase [30]. The aspect ratio of the host rods in the simulations is set such that it roughly matches the effective rod length over diameter ratio of the experimental system, thereby taking into account the electrostatic repulsion of the fd viruses [32].

We equilibrate the system in a low-density Sm_A state using Monte Carlo simulations in an isothermal-isobaric ensemble, i.e., the pressure, temperature, N_g and N_h are kept fixed. Note that the smectic layer spacing in simulations is $\lambda \sim 1.1L_h$, whereas $\lambda \sim 1.0L_{\mathrm{host}}$ in the experimental system of filamentous viruses [32]. After full equilibration we investigate using both standard and dynamic Monte Carlo simulations [33,34] the longitudinal dynamics along the z axis, parallel to the nematic director $\hat{\mathbf{n}}$, for various $L_g \in [0.2, 2.5]L_h$ corresponding to various size ratios $r = (L_g + d)/\lambda$. Within this range of lengths the probability of finding guest rods in a transverse interlamellar configuration is negligible [37,38]. We refer the reader to the Supplemental Material [31] for technical details on the simulations.

In Fig. 1(b), we present typical longitudinal trajectories from both simulations and experiments, showing remarkably similar slow hopping-type dynamics of host particles ($r \sim 1$) as well as fast diffusive behavior of noncommensurate guest particles ($r \sim 1.3$). For each particle trajectory $z(t)$ we measure the mean square displacement along the director $\hat{\mathbf{n}}$, $\mathrm{MSD}(t) = \langle [z(t_0 + t) - z(t_0)]^2 \rangle$, and average

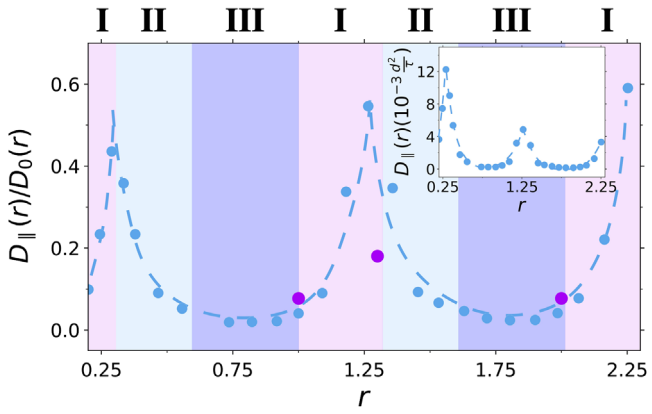

FIG. 2. Longtime diffusion coefficient $D_\parallel(r)$ normalized by the infinite-dilution diffusion coefficient $D_0(r)$ [31] of guest particles as a function of the size ratio r. The experimental values of $D_\parallel(r)$ are shown in purple for $r = 1$, 1.3, and 2 [28]. The inset shows the raw diffusion coefficients. The background is colored according to the three diffusion regimes displayed in Fig. 3, and the dashed lines are guides to the eye.

the MSDs of all particles with equal length. In Fig. 1(c) we show the MSDs for a selected set of size ratios r. For particles with a length commensurate with the smectic layer spacing ($r \sim 1$) we obtain the typical MSD of particles in a lamellar phase [18] with a cage-trapping plateau between the short- and longtime diffusion regimes corresponding to the intralayer and interlayer dynamics, respectively (see Supplemental Material [31]). As the length of the guest particles increases, the time interval for the caging becomes shorter, and eventually disappears for $r \sim 1.25$ when the dynamics becomes nematiclike with a diffusive behavior [Fig. 1(c)]. Upon further increasing the particle length, the cage-trapping plateau reappears ($r \sim 1.45$) and becomes more pronounced as the dynamics becomes hopping-type again for nearly commensurate dimers ($r \sim 1.90$). Similarly, for guest rods shorter than the smectic layer spacing, the time interval of caging decreases ($r \sim 0.47$) and eventually disappears for guest particles of low anisotropy ($r \sim 0.29$).

To quantify the long-term dynamic behavior, we determine the longtime diffusion coefficient $D_\parallel$ defined as half the slope of the MSD at long times, i.e., $\mathrm{MSD}(t) = 2D_\parallel t^\gamma$ (1), and we present $D_\parallel$ normalized by the particle diffusion coefficient at infinite dilution $D_0(r)$ as a function of the size ratio r in Fig. 2. In the range $1 \leq r < 2$, a strong increase of the diffusion is observed with a maximum $D_\parallel(r)/D_0(r)$ at $r \sim 1.25$, corresponding to a fast nematiclike diffusion of particles whose length is not commensurate with the smectic layer spacing. This yields an optimal value for the fastest longitudinal diffusion remarkably close to the particle length ratio for which fast diffusion was observed in experiments [28]. For larger r the diffusion slows down as the hoppinglike dynamics is retrieved. The slowest diffusion is not found for particles twice the length of the smectic layer spacing ($r \sim 2$) but at slightly smaller lengths ($r \sim 1.75$). We also observe in Fig. 2 that the values of $D_\parallel(r)/D_0(r)$ are in good quantitative agreement with the experimental values marked by the purple symbols despite the simplicity of our model. For guest particles shorter than the host ones ($r < 1$), the fastest and the slowest dynamics are obtained by noncommensurate particles of size ratio $r \sim 0.25$ and $r \sim 0.75$ respectively, corresponding to the fast nematiclike diffusion for the former and slow hoppinglike dynamics for the latter. Interestingly, the normalized values for $r < 1$ of the diffusion coefficients for the slowest and fastest dynamics are very similar to their corresponding values for $r > 1$, emphasizing again that the shortest particles do not necessarily diffuse the fastest. In the long rod limit, i.e., for $r > 2$, we find another maximum of $D_\parallel(r)/D_0(r)$ at $r \sim 2.25$.

The dependence of $D_\parallel(r)/D_0(r)$ on the size ratio r in Fig. 2 suggests a periodic behavior of the longitudinal dynamics with a period set by the smectic layer spacing λ. For each size ratio interval $r \in [n, n+1]$ with $n = 0, 1, 2, \ldots$, the dynamics first speeds up as r increases and the smectic caging becomes less severe, reaches a maximum value at $r \simeq n + 0.25$ corresponding to the fastest nematiclike diffusion, and then slows down and reaches a minimal value at $r \simeq n + 0.75$. This periodic behavior can be explained by dividing the end-to-end guest rod length $L_g + d = r\lambda$ into a length $\ell\lfloor r \rfloor$ that is commensurate with $\lfloor r \rfloor$ smectic layers (where the floor function $\lfloor x \rfloor$ denotes the largest integer that is less than x), and an "excess" length of $\ell(r - \lfloor r \rfloor)$. The longitudinal dynamics of guest particles is predominately determined by the excess part of the guest rod, which creates voids in the smectic layers and affects the caging of the lamellar phase. Here, the only effect of the "commensurate" part of the particle is a general slowing down of the dynamics with n (see the inset of Fig. 2).

To quantify the effect of the excess particle length, we measure the effective potential $\beta U_{\mathrm{Sm}}(z) = -\ln[\rho(z)]$ felt by a guest rod, where $\rho(z)$ is the probability distribution of finding a rod-shaped particle in an infinitesimal interval of $[z, z + \delta z]$ and $\beta = 1/k_B T$. The effective potential is periodic due to the smectic host ordering, therefore $\rho(z)$ is only measured in a single smectic layer $0 \leq z < \lambda$. In Figs. 3(a)–3(f), we report the smectic potential for varying length ratios $0 < r < 2$. Surprisingly, we find that the smectic potentials exhibit two barriers, or equivalently two minima at $z_1^{\min}$ and $z_2^{\min}$ which merge into a single minimum when $r \simeq n$, namely when particles are commensurate with the layer spacing. We plot $z_1^{\min}$ and $z_2^{\min}$ for varying r in Fig. 4, allowing us to distinguish three different regimes as schematically illustrated in Fig. 3(g).

In the first regime (I) corresponding to size ratios $r \in [n, n + 0.3]$, the guest particles are on average located at the same position as their commensurate counterparts with $r = n$, i.e., in the middle of the smectic layers. However, as they are longer than $n\lambda$, they create holes in the adjacent smectic layers resulting in a release of the

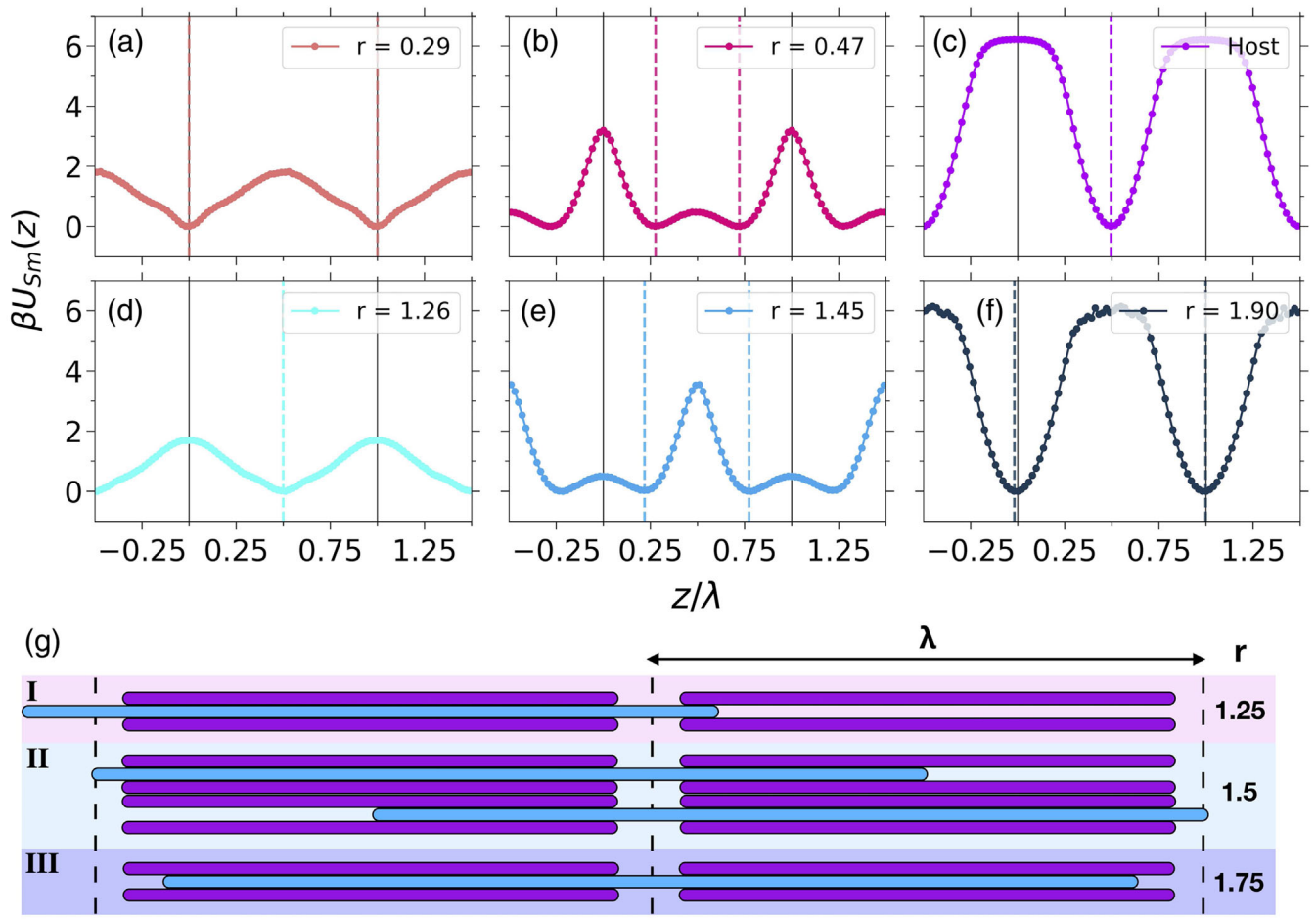

FIG. 3. (a),(f) Effective potential $U_{\mathrm{Sm}}(z)$ experienced by guest particles for varying size ratios $r = (L_g + d)/\lambda$ in a smectic phase with a layer spacing λ. The dashed vertical lines indicate the equilibrium positions of the rod particles, z_1^{min} and z_2^{min}, corresponding to the minima of the ordering potential $U_{\mathrm{Sm}}(z)$. A video showing the variation of $U_{\mathrm{Sm}}(z)$ with the size ratio r can be found in the SM [31]. (g) Sketches of the host (purple) and guest (cyan) particles at their equilibrium positions z_1^{min} and z_2^{min} for three exemplary size ratios ($r = 1.25$, 1.5, 1.75) corresponding to the different diffusion regimes.

cage constraint thereby facilitating the interlayer diffusion and speeding up the dynamics, with the fastest nematiclike diffusion found for $r \sim n + 0.25$. In the opposite limit, the third regime (III) having $r \in [n + 0.6, n + 1]$ exhibits the slowest diffusion behavior and corresponds to guest particles which already have the same equilibrium position as the next commensurate multimer ($r = n + 1$). Because the guest rods are shorter than $(n + 1)\lambda$, they first have to diffuse within the smectic layer to reach one of its two boundaries, before they can jump to the adjacent layer, slowing down the longitudinal diffusion in comparison to the one associated with commensurate particles. We denote regime III as the slow diffusive regime. More intriguingly perhaps is the regime II with $r \in [n + 0.3, n + 0.6]$, where the minima z_1^{min} and z_2^{min} correspond to the center-of-mass positions at which one of the ends of the guest particles touches one of the boundaries of the smectic layers [Figs. 3(b) and 3(e)]. This was recently experimentally observed for short rods dispersed in colloidal monolayer of host rod-shaped particles with a length ratio $r \sim 0.5$ [39]: the short rods were found to strongly anchor to the membrane interfaces, and only occasionally hop to the opposite interface. Our results confirm this anchoring

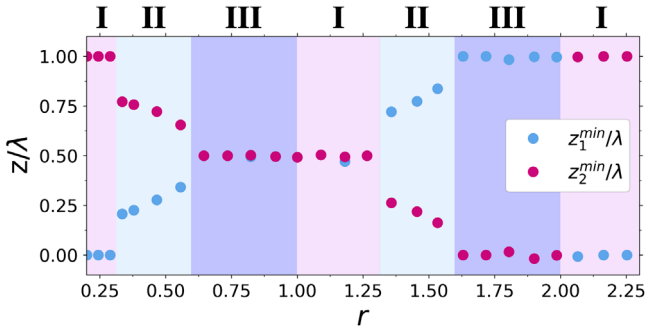

FIG. 4. Center-of-mass positions z_1^{min} and z_2^{min} of the guest rods corresponding to the minima of the effective smectic potential as a function of size ratio r. The background is colored according to the three diffusive regimes displayed in Fig. 3.

behavior and extend it to particles even larger than the lamellar spacing. The preferential adsorption of noncommensurate guest rods at the interface of smectic layers can be explained by the fact that guest rods at the interface generates large voids that can be partially filled via small angular fluctuations of neighboring host particles, thereby hindering their diffusion. However, if the guest particle is at the center of a smectic layer (or in between two smectic layers), the resulting voids are smaller, making it harder for host particles to occupy the empty space. This would indeed require a higher tilt angle of the host rods, hence generating a defect structure in the smectic organization. As a consequence, the guest particles escape from this central position and adhere to one of the two smectic layer interfaces. In this regime II, referred as the switching regime, the guest particles experience two potential barriers of varying height [Figs. 3(b) and 3(d)] for varying r, which results from a nontrivial interplay of the effective smectic potentials that are felt by single host rods [$r \sim 1$, Fig. 3(c)] as well as by commensurate rods [$r \sim 2$, Fig. 3(f)] and which are out-of-phase in terms of barrier locations (see Supplemental Material [31]).

In conclusion, we showed that the dynamics of guest rods can be controlled by tuning the ratio r of their size over the lamellar spacing. We observed that the longtime diffusion coefficient $D_{\parallel}$ is a periodic function of r, as the longitudinal dynamics is entirely determined by the excess length $\ell(r - \lfloor r \rfloor)$ of the guest particle. We show that this behavior can be rationalized by a 1D effective periodic potential exhibiting up to two energy barriers, yielding a slow, an intermediate and a fast diffusive regime, granting complete control over the type and speed of the dynamics of guest particles in a smectic environment.

M. C. and M. D. acknowledge financial support from the EU H2020-MSCA-ITN- 2015 project MULTIMAT (Marie Sklodowska-Curie Innovative Training Networks) [Project No. 676045].

*m.chiappini@uu.nl
†m.dijkstra@uu.nl

[1] T. Nagatani, Rep. Prog. Phys. **65**, 1331 (2002).
[2] E. R. Weeks and D. A. Weitz, Chem. Phys. **284**, 361 (2002).
[3] W. C. K. Poon, MRS Bull. **29**, 96 (2004).
[4] P. Chaudhuri, L. Berthier, and W. Kob, Phys. Rev. Lett. **99**, 060604 (2007).
[5] P. R. Smith, I. E. G. Morrison, K. M. Wilson, N. Fernández, and R. J. Cherry, Biophys. J. **76**, 3331 (1999).
[6] I. Golding and E. C. Cox, Phys. Rev. Lett. **96**, 098102 (2006).
[7] J. A. Dix and A. S. Verkman, Annu. Rev. Biophys. **37**, 247 (2008).
[8] I. M. Sokolov, Soft Matter **8**, 9043 (2012).
[9] M. P. B. van Bruggen, H. N. W. Lekkerkerker, G. Maret, and J. K. G. Dhont, Phys. Rev. E **58**, 7668 (1998).
[10] H. Löwen, Phys. Rev. E **59**, 1989 (1999).
[11] M. P. Lettinga, E. Barry, and Z. Dogic, Europhys. Lett. **71**, 692 (2005).
[12] A. M. Alsayed, M. F. Islam, J. Zhang, P. J. Collings, and A. G. Yodh, Science **309**, 1207 (2005).
[13] B. van der Meer, W. Qi, R. G. Fokkink, J. van der Gucht, M. Dijkstra, and J. Sprakel, Proc. Natl. Acad. Sci. U.S.A. **111**, 15356 (2014).
[14] B. van der Meer, M. Dijkstra, and L. Filion, J. Chem. Phys. **146**, 244905 (2017).
[15] S. Belli, A. Patti, R. van Roij, and M. Dijkstra, J. Chem. Phys. **133**, 154514 (2010).
[16] S. Naderi, E. Pouget, P. Ballesta, P. van der Schoot, M. P. Lettinga, and E. Grelet, Phys. Rev. Lett. **111**, 037801 (2013).
[17] M. P. Lettinga and E. Grelet, Phys. Rev. Lett. **99**, 197802 (2007).
[18] R. Matena, M. Dijkstra, and A. Patti, Phys. Rev. E **81**, 021704 (2010).
[19] E. Pouget, E. Grelet, and M. P. Lettinga, Phys. Rev. E **84**, 041704 (2011).
[20] A. Patti, D. E. Masri, R. van Roij, and M. Dijkstra, J. Chem. Phys. **132**, 224907 (2010).
[21] R. W. Ruhwandl and E. M. Terentjev, Phys. Rev. E **54**, 5204 (1996).
[22] H. Stark and D. Ventzki, Phys. Rev. E **64**, 031711 (2001).
[23] J. C. Loudet, P. Hanusse, and P. Poulin, Science **306**, 1525 (2004).
[24] K. Kang, J. Gapinski, M. P. Lettinga, J. Buitenhuis, G. Meier, M. Ratajczyk, J. K. G. Dhont, and A. Patkowski, J. Chem. Phys. **122**, 044905 (2005).
[25] F. Mondiot, J.-C. Loudet, O. Mondain-Monval, P. Snabre, A. Vilquin, and A. Würger, Phys. Rev. E **86**, 010401(R) (2012).
[26] T. Turiv, I. Lazo, A. Brodin, B. I. Lev, V. Reiffenrath, V. G. Nazarenko, and O. D. Lavrentovich, Science **342**, 1351 (2013).
[27] A. Martinez, P. J. Collings, and A. G. Yodh, Phys. Rev. Lett. **121**, 177801 (2018).
[28] L. Alvarez, M. P. Lettinga, and E. Grelet, Phys. Rev. Lett. **118**, 178002 (2017).
[29] P. Bolhuis and D. Frenkel, J. Chem. Phys. **106**, 666 (1997).
[30] E. Grelet, Phys. Rev. Lett. **100**, 168301 (2008).
[31] See Supplemental Material at http://link.aps.org/supplemental/10.1103/PhysRevLett.124.087801, which includes details on the computational methods and on the conversion between computational and experimental time units, the caging time that a particle typically spend within a smectic layer as a function of its length, a discussion of the mechanism driving the adsorption to the smectic layer interfaces in the intermediate switching regime, and the potential barriers of the effective smectic potential as a function of r. The discussion includes Refs. [28,32–36].
[32] E. Grelet, Phys. Rev. X **4**, 021053 (2014).
[33] A. Patti and A. Cuetos, Phys. Rev. E **86**, 011403 (2012).

[34] A. Cuetos and A. Patti, Phys. Rev. E **92**, 022302 (2015).
[35] D. Frenkel and B. Smit, *Understanding Molecular Simulation: From Algorithms to Applications* (Elsevier, San Diego, 2001).
[36] M. M. Tirado and J. G. de la Torre, J. Chem. Phys. **71**, 2581 (1979).
[37] R. van Roij, P. Bolhuis, B. Mulder, and D. Frenkel, Phys. Rev. E **52**, R1277 (1995).
[38] J. S. van Duijneveldt and M. P. Allen, Mol. Phys. **90**, 243 (1997).
[39] M. Siavashpouri, P. Sharma, J. Fung, M. F. Hagan, and Z. Dogic, Soft Matter **15**, 7033 (2019).

Supplemental Material

Massimiliano Chiappini, Eric Grelet, and Marjolein Dijkstra

(Dated: January 30, 2020)

I. COMPUTATIONAL METHODS

We model the experimental mixture of host and guest fd-viruses as a binary mixture of hard spherocylinders. We perform Monte Carlo simulations on a binary mixture of $N_h = 3072$ host rods of length L_h and diameter d and $N_g = 6$ guest rods of length L_g and diameter d. We use a high-density ABC crystal state as our initial configuration, and we expand the system via Monte Carlo (MC) simulations in the NPT ensemble to a low-density smectic state at pressure $\beta P v_0 \approx 6.39$ with a smectic layer spacing $\lambda \sim 1.1 L_h$. We keep the number of particles, N_g and N_h, the pressure P, and the temperature T fixed in the NPT MC simulation, whereas the system volume V and the particle configurations (positions and orientations) are evolved via random variations that are either accepted or rejected according to the acceptance rules that enforce the correct statistical physics [1].

After equilibration of the system, we perform production runs in the NVT ensemble, i.e. the number of particles N, volume V, and hence the density $\rho = N/V$ are kept fixed, and we track the positions of 3000 host particles and 6 guest particles to measure their diffusive properties. In general, MC simulations are not guaranteed to yield realistic particle trajectories, and do not provide a physical time scale. However, for sufficiently small maximum displacements NVT-MC simulations with simple translational and rotational moves produce trajectories that follow the correct Brownian dynamics. In the case of anisotropic particles, the maximum displacements have to be tuned according to the self-diffusion properties of each particle in order to enforce the correct anisotropy of the dynamics. More specifically, for rod-like particles, the ratio between the maximum displacements parallel and perpendicular to the particle axis $\delta_\parallel/\delta_\perp$ has to be equal to the ratio between the parallel and perpendicular diffusion coefficients at infinite dilution $D_{0,\parallel}/D_{0,\perp}$ [2].

In this Letter, we study the dynamic behavior of guest rods in a host smectic environment parallel to the nematic director $\hat{\mathbf{n}}$. However, reaching the long-term diffusive regime of highly anisotropic particles in a smectic phase is a highly non-trivial computational effort. In order to reach and explore the long-term regime of the longitudinal dynamics of guest particles in a reasonable computational time, we increase the ratio between the parallel and perpendicular maximum displacements to speed up the parallel diffusion relative to the perpendicular one. Here, we assume that the parallel and perpendicular dynamics can be decoupled, *i.e.* that the perpendicular diffusive behavior has a negligible effect on the parallel diffusion. In

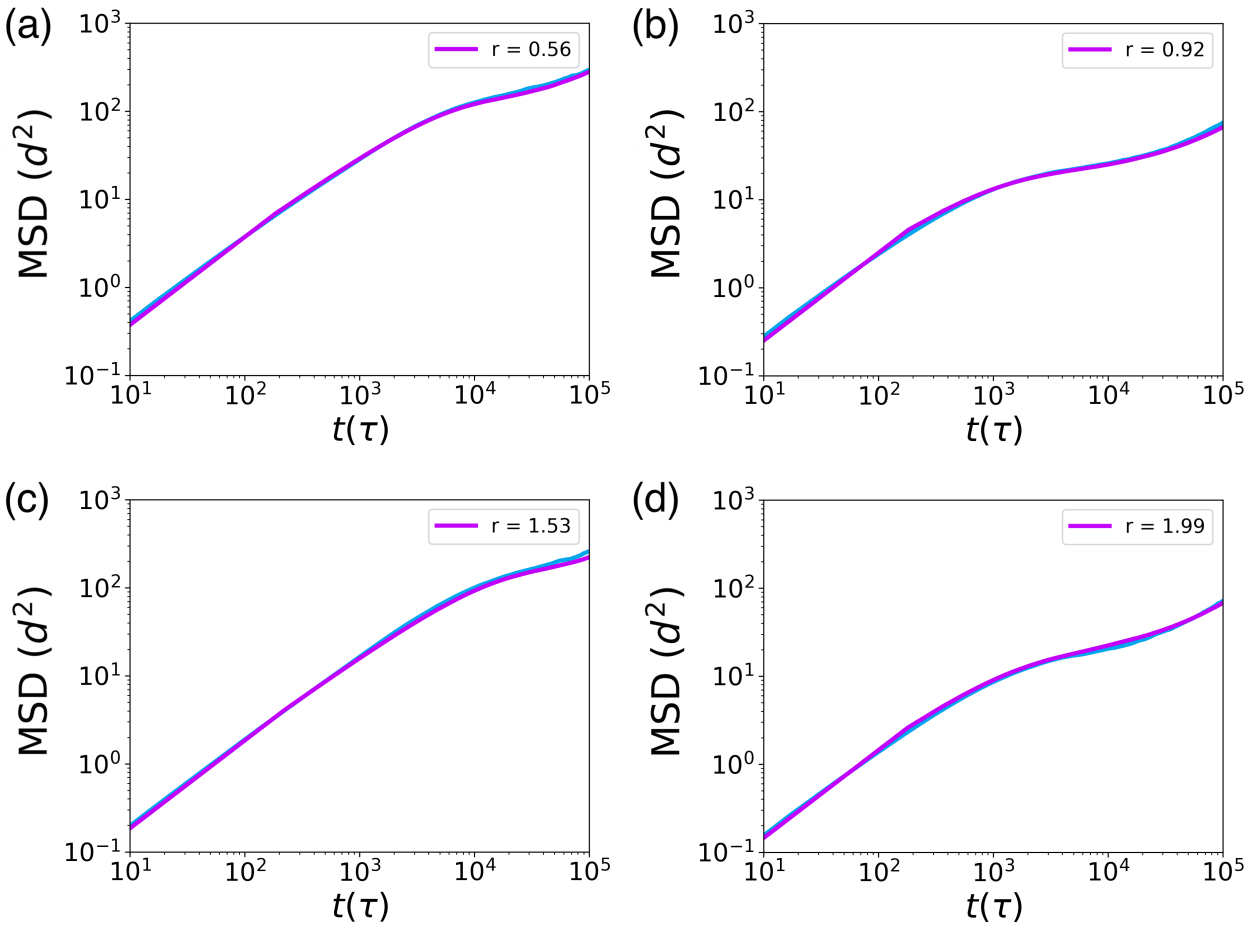

FIG. S1. Parallel MSDs (along the long rod axis) in the smectic-A phase from basic MC simulations (in purple) after rescaling onto the MSDs from DMC simulations (in blue) for size ratios $r = 0.56$ (a), 0.92 (b), 1.53 (c), and 1.99 (d).

particular, we set $\delta_\perp = 0.08d$ and $\delta_\parallel = 5\delta_\perp = 0.4d$, and we find that for these values of the maximum displacements, MC simulations consisting of $\sim 1.5 \cdot 10^8$ MC cycles are sufficient to reach and adequately sample the long-term diffusive behavior. In particular, we save the positions of the tracked host and guest particles every 10^3 MC steps, hence producing trajectories of $N_t \sim 1.5 \cdot 10^5$ points.

We measure the MSD at discrete times $t \in [1, N_t]$ using N_g trajectories $z_i = [z_{i,1}, z_{i,2}, \ldots, z_{i,N_t}]$ as

$$MSD(t) = \frac{1}{N_g} \sum_{i=1}^{N_g} \frac{1}{(N_t - t)} \sum_{j=1}^{N_t - t} \left(z_{i,(j+t)} - z_{i,j} \right)^2 . \tag{1}$$

In order to determine the long-term diffusion coefficient $D_\parallel$, we consider a wide collection of time windows $\{[t_0, t_1]\}$ in the long-time diffusion limit of the MSD. In each time window,

we perform a fit of the MSD with $\gamma = 1$, and measure the reduced χ^2. Subsequently, we average the values of D of all time windows for which χ^2 is smaller than a certain threshold value. The statistical error on D is determined as the standard error on the average, and is of about the symbol size or smaller as indicated in Fig. 2 of the letter.

To test the validity of our assumption on the decouping of the parallel and perpendicular dynamics, we compare the MSDs from our MC simulations and the ones from simulations performed using the Dynamic Monte Carlo (DMC) method introduced by Patti and Cuetos [3]. In the DMC method, the maximum displacements of both translational and rotational motions are carefully tuned according to the diffusive properties of the particles at infinite dilution, resulting in reliable Brownian dynamics with respect to a physical unit of time $\tau = \mu\sigma^3/k_BT$, where μ is the solvent viscosity, σ the characteristic unit of length in the system and T the solvent temperature. We note that in the case of a binary mixture (as our guest/host particles mixture) a specific treatment is required as discussed in Ref. [4]. For every length of our guest particle that we consider, we perform an additional simulation with the more accurate but slow DMC method. Subsequently, we map the short-time MSDs from our basic MC simulations onto the ones from DMC simulations by rescaling the unit of time. If this mapping is accurate, the dynamics using the basic MC simulations is sufficiently reliable, and the rescaling of time onto the physical time unit τ can be used to compare the dynamical properties with experiments. In Fig. S01 we show typical examples of such a rescaling for varying size ratios $r = (L_g + d)/\lambda$ of the guest rods with λ the smectic layer spacing confirming the good mapping between the two approaches.

II. COMPUTATIONAL AND EXPERIMENTAL TIMES

In Fig. 1b of the Letter, we compare typical longitudinal trajectories of host and guest particles from simulations and experiments on the same time scale. However, matching the experimental and computational time scales is non-trivial, and deserves some discussion.

In the Section above we already showed that the mapping of the MSDs obtained from basic MC simulations onto DMC simulations provides a physical time unit $\tau = \mu\sigma^3/k_BT$, where μ is the solvent viscosity, σ the unit of length, and T the solvent temperature. In the experiments of Ref. [5], the particles are dispersed in water at room temperature, for which $\mu = 10^{-3}$ Pa $\cdot$ s and $k_BT = 4.11 \cdot 10^{-21}$ J. In our simulations, we use the particle diameter

d as our unit of length, and hence in the experimental system σ corresponds to the effective diameter $d_{eff} \sim 20$ nm of the fd viruses, where we have taken into account the electrostatic repulsion between the charged viruses [6]. This results in a conversion factor $\tau \approx 2 \cdot 10^{-6}$ s.

To test this conversion factor, we perform DMC simulations of single particles and measure their infinite dilution diffusion coefficient $D_0^{sim} = 1.16 \cdot 10^{-2} d^2/\tau$. Theoretically, the diffusion coefficient D_0^{th} of long rods ($L/d \ggg 1$) at infinite dilution is known and is expressed as [2]:

$$D_0^{\text{th}} = \frac{k_B T}{3\pi\mu L} \ln\left(\frac{L}{d}\right). \tag{2}$$

This yields for rods with an aspect ratio of $L/d \sim 40$, a diffusion coefficient $D_0^{\text{th}} = 2.3\ \mu\text{m}^2/\text{s}$, which is in quantitative agreement with $D_0^{\text{exp}} \approx 2\mu\text{m}^2/\text{s}$ experimentally measured in very dilute filamentous virus suspensions. Considering that $d = 20$ nm, with $\tau = 2 \cdot 10^{-6}$ s, we obtain $D_0^{sim} = 2.3\ \mu\text{m}^2/\text{s} = D_0^{\text{th}} \approx D_0^{\text{exp}}$, confirming the value of our conversion factor.

III. CAGING TIMES

As discussed in the Letter, the typical longitudinal MSD of a rod-like particle in a smectic environment is characterised by a cage-trapping plateau in between the short- and long-time diffusion regimes. We measure the extent of the caging effect upon varying the size ratio r of the guest particle with respect to the smectic layer spacing. Given the MSD across the three timescales for a given particle length, we perform three separate fits of the short-, intermediate-, and long-time regimes of the MSD. At short and long times, we fit the MSD with the theoretical expression for diffusive dynamics, $\text{MSD}(t) = 2Dt$, whereas at intermediate time we fit it with the expression for subdiffusive dynamics, $\text{MSD}(t) = 2Dt^\gamma$ with $\gamma < 1$. From the interception points between the fits at short and intermediate times, and the fits at intermediate and long times, we estimate the typical caging time δt, as shown in Fig. S02.

In Fig. S03 we report the caging time δt as a function of size ratio r. It clearly shows the opposite trend as the diffusion coefficients shown in the inset of Fig. 3 of the Letter, confirming the relationship between the shrinking of the caging plateau and the speeding up of the dynamics.

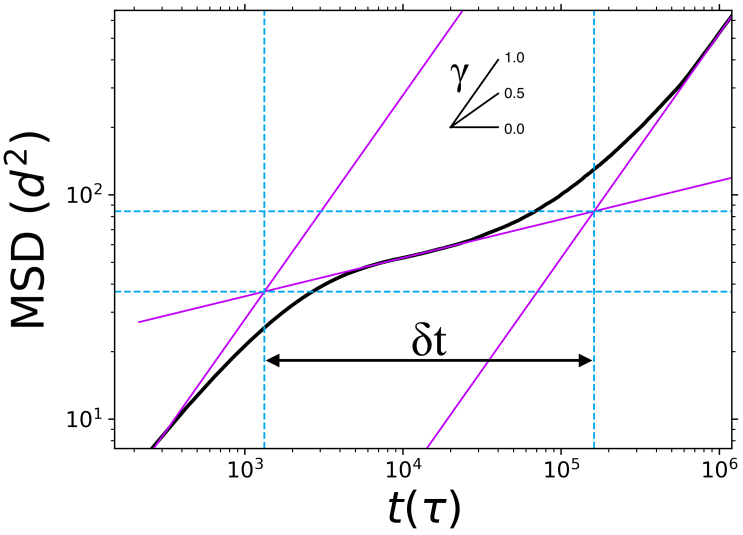

FIG. S2. MSD (in black) of guest rods with a size ratio $(L_g + d)/\lambda = 0.73$ in a host smectic environment with a smectic layer spacing λ with fits (in purple) of the short-, intermediate-, and long-time diffusion regimes. From the intercepts of the fits, we identify the time regimes in which the dynamics switches between short-time diffusion to an intermediate-time caged sub-diffusion with a caging time δt, to a long-time diffusion.

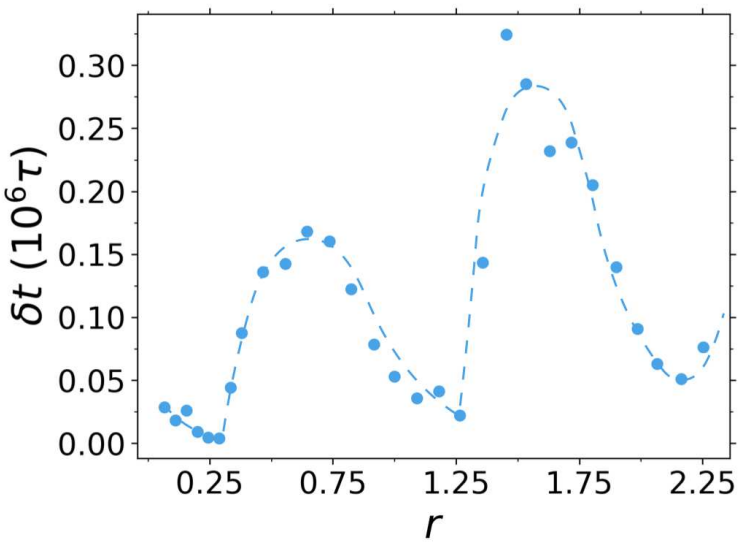

FIG. S3. Caging times δt as a function of the size ratio $r = (L_g + d)/\lambda$ of the guest particles. The dashed line is a guide to the eye.

IV. ADSORPTION TO THE INTERFACE OF THE SMECTIC LAYERS

Most of the smectic potentials presented in the Letter have a characteristic shape with two minima, implying that guest particles have two equilibrium positions (regime II). In particular, as shown in the Letter, these minima correspond to positions in which either one of the particle ends is adhered to the interface of a smectic layer.

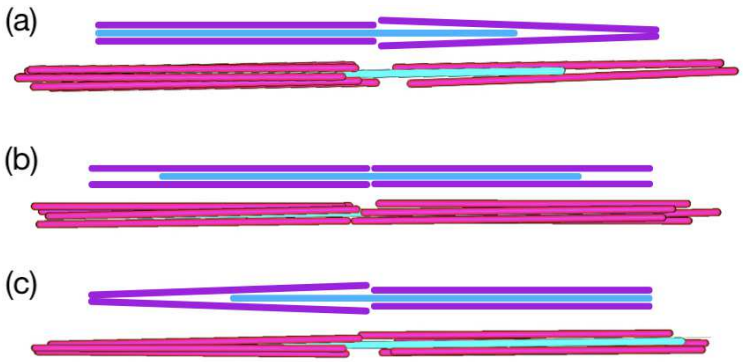

FIG. S4. Sketches (top) and snapshots from actual simulations (bottom) of a guest particle of length $L_g = 1.5L_h$ (corrisponding to a size ratio $r \sim 1.36$) and its neighbour host particles (whose centre of mass is contained in a cylinder of diameter $3D$ and height 3λ around the guest particle). When the guest particle adheres to an interface between layers (a and c) the voids created in the adjacent layer are wide enough for host particles to occupy it and to hinder the diffusion of the guest particle. Vice versa, when the particle sits in the center of a smectic layer (b), it creates two voids which are too small to be populated by host particles and hence the guest particle can diffuse away freely.

Fig. 4a-f of the main text shows that the two minima $z_1^{\min}$ and $z_2^{\min}$ of the effective potentials are separated by two potential barriers located at $z = n\lambda$ (barrier A) and $z = (n + 1/2)\lambda$ (barrier B). Monomers and "odd" multimers with $r \sim (2n + 1)$ feel exclusively the barriers at $z = n\lambda$, and dimers and "even" multimers with $r \sim (2n + 2)$ experience only the barriers at $z = (n + 1/2)\lambda$. As shown in Fig. S5a, guest particles in regime I experience exclusively the same barrier as the preceding multimer, whereas in regime III they only feel the same barrier as the successive multimer. In regime II, the dynamics of the guest rods is affected by both barriers and switches from a "monomer"-like to a "dimer"-like behavior upon changing r. Interestingly, in Fig. S5b we find that the sum of the barriers, accounting for the total smectic caging felt by the guest particle, is minimal for $r \sim n + 0.25$, for which

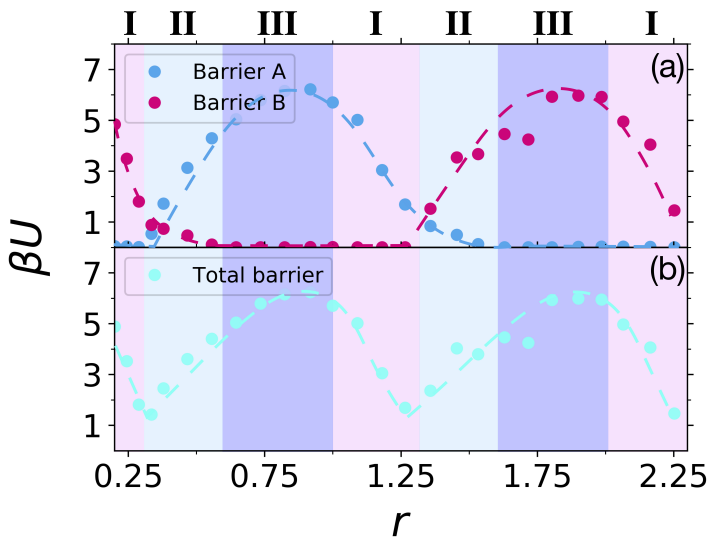

FIG. S5. (a) Height and (b) sum of the two potential energy barriers as a function of the size ratio r for guest rods in a host smectic phase. The background is colored according to the three diffusive regimes. Dashed lines are guides to the eye.

the fastest dynamics is observed, and maximal for $r \sim n + 0.75$, when the slowest dynamics is achieved, confirming that the dynamic behavior of guest rods in a host smectic phase can be rationalized in terms of the caging due to the lamellar environment

[1] D. Frenkel and B. Smit, *Understanding molecular simulation: from algorithms to applications* (Elsevier, 2001).

[2] M. M. Tirado and J. G. de la Torre, The Journal of Chemical Physics **71**, 2581 (1979).

[3] A. Patti and A. Cuetos, Phys. Rev. E **86**, 011403 (2012).

[4] A. Cuetos and A. Patti, Phys. Rev. E **92**, 022302 (2015).

[5] L. Alvarez, M. P. Lettinga, and E. Grelet, Phys. Rev. Lett. **118**, 178002 (2017).

[6] E. Grelet, Phys. Rev. X **4**, 021053 (2014).